

Supplementary Information

Curtailing Perovskite Processing Limitations via Lamination at the Perovskite/Perovskite Interface

*Sean P. Dunfield^{1,2,3}, David T. Moore¹, Talysa R. Klein¹, David M. Fabian^{1,6}, Jeffrey A. Christians¹, Alex G. Dixon^{1,2}, Benjia Dou^{1,5}, Shane Ardo^{6,7}, Matthew C. Beard¹, Sean E. Shaheen^{2,4,5}, Joseph J. Berry^{1,2,4 *}, Maikel F.A.M. van Hest^{1,*}*

National Renewable Energy Laboratory, Golden, CO 80401¹

Renewable and Sustainable Energy Institute, University of Colorado Boulder, Boulder, CO
80309²

Materials Science & Engineering Program, University of Colorado Boulder, Boulder, CO 80309³
Department of Physics, University of Colorado Boulder, Boulder, CO 80309⁴

Department of Electrical, Computer and Energy Engineering, University of Colorado Boulder,
Boulder, CO 80309⁵

Department of Chemistry, University of California Irvine, Irvine, CA 92697⁶

Department of Chemical Engineering and Materials Science, University of California Irvine,
Irvine, CA 92697⁷

Corresponding Authors*: maikel.van.hest@nrel.gov, joe.berry@nrel.gov

Experimental

Chemicals: MAI was purchased from Dyesol. PbI₂ (99.9985%) and SnO₂ (15% in H₂O colloidal dispersion) were purchased from Alfa Aesar. All other chemicals and solvents were obtained from Sigma-Aldrich and used as received.

Substrate Preparation: Full FTO TEC 15 sheets were ordered from Hartford Glass Co. and cut down to 1 x 1 in using a diamond scribe. The substrates were then pattered film-side-up as shown in Figure S1 with a Q-switched 532 nm Nd:YVO₄ laser scribe at 100 mm/s utilizing a 40 μm beam diameter, 30 A of current, and a 0.02 mm beam overlap. Once etched, the substrates were immediately cleaned with lint free clean room wipes and set aside until needed. Prior to deposition, the substrates were sonicated in acetone, isopropanol alcohol, and deionized water for 15 min each, and then UV-ozone treated for 15 min.

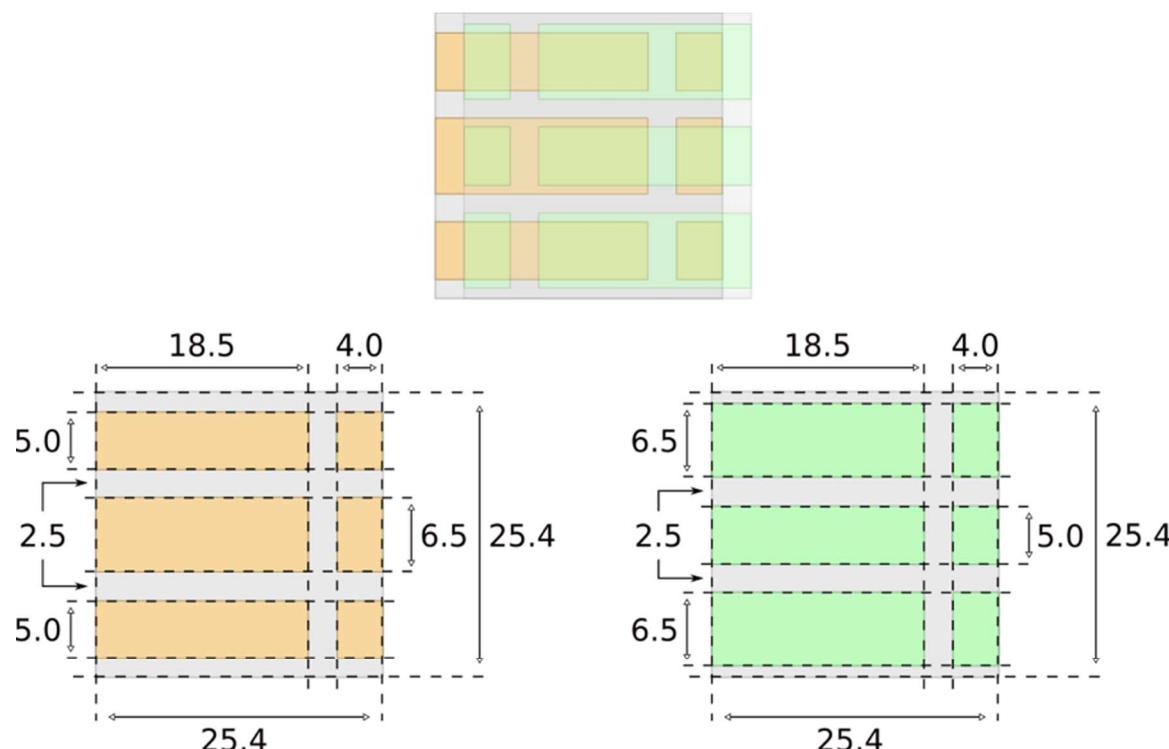


Figure S1. Substrate design (top) and corresponding TCO patterns (bottom) utilized for devices.

Nickel Oxide (NiO_x): Nickel oxide films were created following a procedure modified from that of You *et al.*¹ The recipe utilized here differs in its use of an intermediate cooling step to reduce the dispersity of nanoparticles and shorter spin time to minimize differences seen from the first to last sample due to the two-part annealing utilized. First, nickel nitrate hexahydrate ($\text{Ni}(\text{NO}_3)_2 \cdot 6\text{H}_2\text{O}$) was fully dissolved in ethylene glycol to form a 1 M solution. The solution was then placed in a freezer. Roughly 30 min before deposition, the green-colored solution was removed from the freezer, 1 M of ethylenediamine was added, and the vial was quickly agitated by vortexing, causing the solution to turn dark blue. The solution was then sonicated for 5 min, deposited through a 0.2 um PTFE filter, and spun cast at 5000 rpm for 45 secs with a ramp time of 1 sec. Samples were then placed on a hotplate at 100 °C and when all samples were on the hotplate, the hotplate was ramped to 300 °C, where it was kept for an hour. Once fully annealed, the samples were removed and loaded into a glovebox as quickly as possible for perovskite deposition.

Tin Oxide (SnO_x): Tin oxide films were fabricated following a procedure reported by Jiang *et al.*² Briefly, SnO_2 (15% in H_2O colloidal dispersion) was diluted to 2.67% using deionized water and then sonicated for 10 min in cold water. Soon after, the solution was spun cast onto the substrates at 3000 rpm for 30 secs with a 1 sec ramp rate. A PTFE filter was not used because the alkaline nature of the solution degrades PTFE. The cast films were then annealed on a hot plate for 30 min at 150 °C in air and then cleaned by UV-ozone treatment for 15 min immediately before perovskite film deposition.

Methylammonium Lead Iodide (MAPI) Perovskite: Perovskite films were created based on a procedure reported by Noel *et al.*³ Because the thickness of the perovskite layer doubles in

lamination, slightly different molarities and solvent ratios were utilized to obtain thinner films. In short, a 25% methylamine (MA) in acetonitrile (ACN) stock solution was prepared by slowly condensing pure MA into a round-bottom flask of ACN at -15 °C. To prevent degradation, this stock solution was kept in a freezer at -5 °C until use. MAI and PbI₂ were then weighed out in a 1.00:1.04 mole ratio. Next, pure anhydrous ACN and stock MA in ACN were added to the perovskite precursors in a 7:9 volume ratio to obtain a 0.5 M solution. This solution was then deposited onto substrates through a 0.2 µm PTFE filter and spun cast at 2500 rpm for 30 sec with a ramp time of 1 sec. Finally, coated films were annealed at 100 °C for 20 min to allow drying. All solution synthesis was done in air, while all deposition and annealing was performed in an argon-filled glovebox.

Lamination/Delamination Procedure: A glass/FTO/SnO_x/perovskite half stack and glass/FTO/NiO_x/perovskite half stack were sandwiched perovskite-to-perovskite between two PTFE release liners and on top of a PTFE mesh (setup shown in Figure S2). A deformable silicon membrane was then cut to size and placed above the release liner where the two half stacks overlap. The silicon membrane/PTFE release liner/top half stack/bottom half stack/PTFE release liner/PTFE mesh stack was then placed between two more release liners and underneath a die press in a carver hydraulic hot press at ~ 300 psi and 150 °C for 20 min. Note that the natural compression/elasticity of the pads causes pressure to naturally decrease over the lamination duration. To ensure that pressure remained uniform for the initial 5 min, pressure was slowly applied to match any drops in pressure. Once the allotted time was complete, pressure was released over the course of ~2 min before the device membrane sandwich was removed. Finally, after allowing the stack to cool for another minute, the release liners, PTFE mesh, and silicone membrane were detached to yield the final device. This procedure produced optimal pressure

uniformity. Subsequent delamination at the SnO_x /perovskite interface was achieved by forcibly twisting each overhanging edge in the opposite direction.

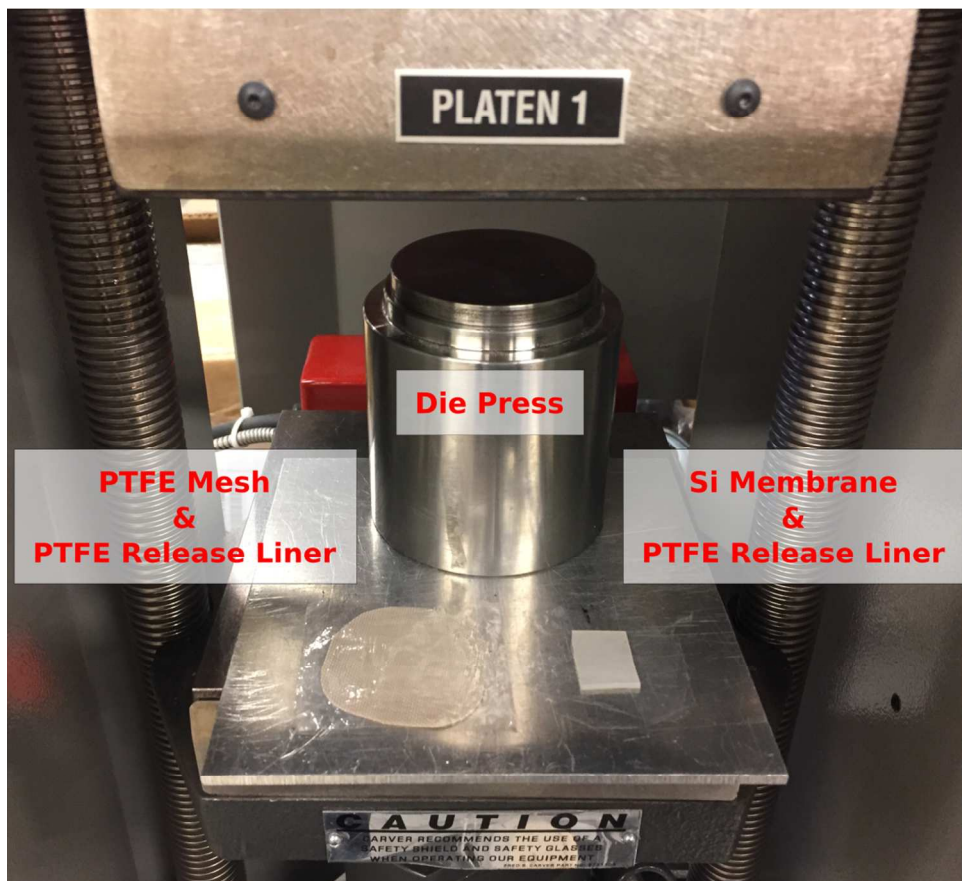


Figure S2. Carver hot press, die press, PTFE mesh, PTFE release liner, and silicon membrane utilized to obtain uniform pressure and heat during lamination.

UV–Vis Absorption: Transmission and reflection spectra were obtained using an integrating sphere in a Shimadzu UV-3600 ultraviolet-visible-near-infrared spectrophotometer. Absorption was calculated by assuming $\text{Absorptance} = 1 - \text{Transmittance} - \text{Reflectance}$. The contribution of each glass/FTO/transportation material layer was then subtracted out and values were converted to absorbance. The correction for the back substrate of the laminated device was taken film-first in an attempt to accurately mimic the path of light, although using data from the other face of the

film yields qualitatively identical conclusions. To compare the curves, spectra were normalized at 725 and 825 nm. This was done by performing baseline subtraction at 825 nm, where the perovskite does not absorb, and then normalizing spectra at 725 nm, away from the band edge of the perovskite, using scalar multiplication.

External Quantum Efficiency (EQE): To compare the external quantum efficiencies, two complete devices were required. The laminated device was produced as described above. The FTO/SnO_x/MAPI/spiro-OMeTAD/MoO_x/Al device was fabricated by completing a FTO/SnO_x/MAPI half stack with spiro and MoO_x/Al as reported by Dou *et al.*⁴ In short, a spiro-OMeTAD solution consisting of 72 mg/mL spiro-OMeTAD, 0.028 mL/mL 4-tert-butylpyridine, and 0.017 mL/mL of a 520 mg/mL bis(trifluoromethanesulfonyl)imide lithium salt (Li-TFSI) in ACN solution was deposited onto the half-stacks at 3000 rpm for 30 sec with a ramp rate of 1 sec. The films were then left to dry and oxidize overnight before 15 nm of MoO_x and 150 nm of Al were thermally evaporated at 0.1 nm/s and 1 nm/s respectively to finish the device. Both devices were analyzed using an Oriel IQE 200 system. Due to the active area being a similar size to the spot size, several measurements were conducted, and the highest performing curve was used for analysis to ensure proper alignment. To compare the curves, spectra were again normalized at 825 and 725 nm as done for absorption measurements; specifically, baseline subtraction was performed at 825 nm (where the perovskite does not absorb) and then spectra were normalized at 725 nm (away from the band edge of the perovskite) using scalar multiplication.

X-Ray Diffraction (XRD): XRD data were recorded on a Bruker D8 Discover X-ray diffractometer with a Hi-Star 2D area detector using Cu K α radiation (1.54 Å). Samples were scanned for 30 min with an x-y raster of 5 mm. To obtain the 2-D graphs displayed, 3-D images

were integrated along phi. To compare the curves, spectra were normalized. This was done by performing baseline subtraction and then normalizing the most intense peak of each spectrum using scalar multiplication.

Atomic Force Microscopy (AFM): AFM images were acquired on an Asylum Research MFP-3D AFM operating in contact mode in ambient conditions. A μ masch HC:CSC17/No Al tip with a nominal tip radius of \sim 8 nm and nominal cantilever stiffness of 0.18 N/m was used to acquire 5 μ m by 5 μ m images with a resolution of 256 data points per line. The images were leveled by mean plane subtraction and flattened line-by-line using Gwyddion image analysis software.⁵ Surface roughness was measured as the root mean-squared roughness over the scan area. As can be seen in Figure S3, MAPI films grown on both (a) SnO_x and (b) NiO_x are extremely smooth, with RMS values of 9.63 nm and 9.44 nm respectively.

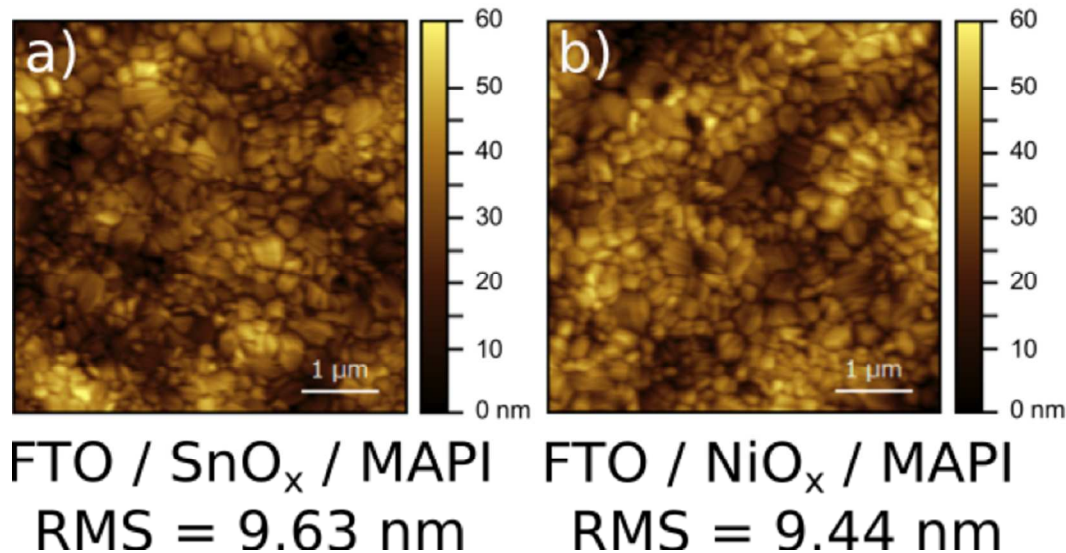


Figure S3. Atomic Force Microscopy images of (a) FTO/ SnO_x /MAPI and (b) FTO/ NiO_x /MAPI half stacks with corresponding route mean-squared surface roughness measurements. Note that the perovskite recipe used forms extremely smooth films.

Scanning Electron Microscope (SEM): In order to provide another metric to judge the effects of lamination, cross sectional SEM images of pre-laminated and delaminated stacks are included. Samples were cleaved, coated with carbon electrodag paint to minimize charging, and quickly loaded into a FEI Nova NanoSEM 630 for analysis using a 3keV beam with 40 μA of current at a working distance of 4-6 μm . Figure S4 shows cross sectional SEM images obtained for (a) FTO/SnO_x/MAPI pre-laminated half-stack, (b) FTO/NiO_x/MAPI pre-laminated half-stack, (c) FTO/SnO_x delaminated half, and (d) FTO/NiO_x/MAPI/MAPI delaminated half. These results show that structural evolution occurs at the MAPI/MAPI interface during the lamination process.

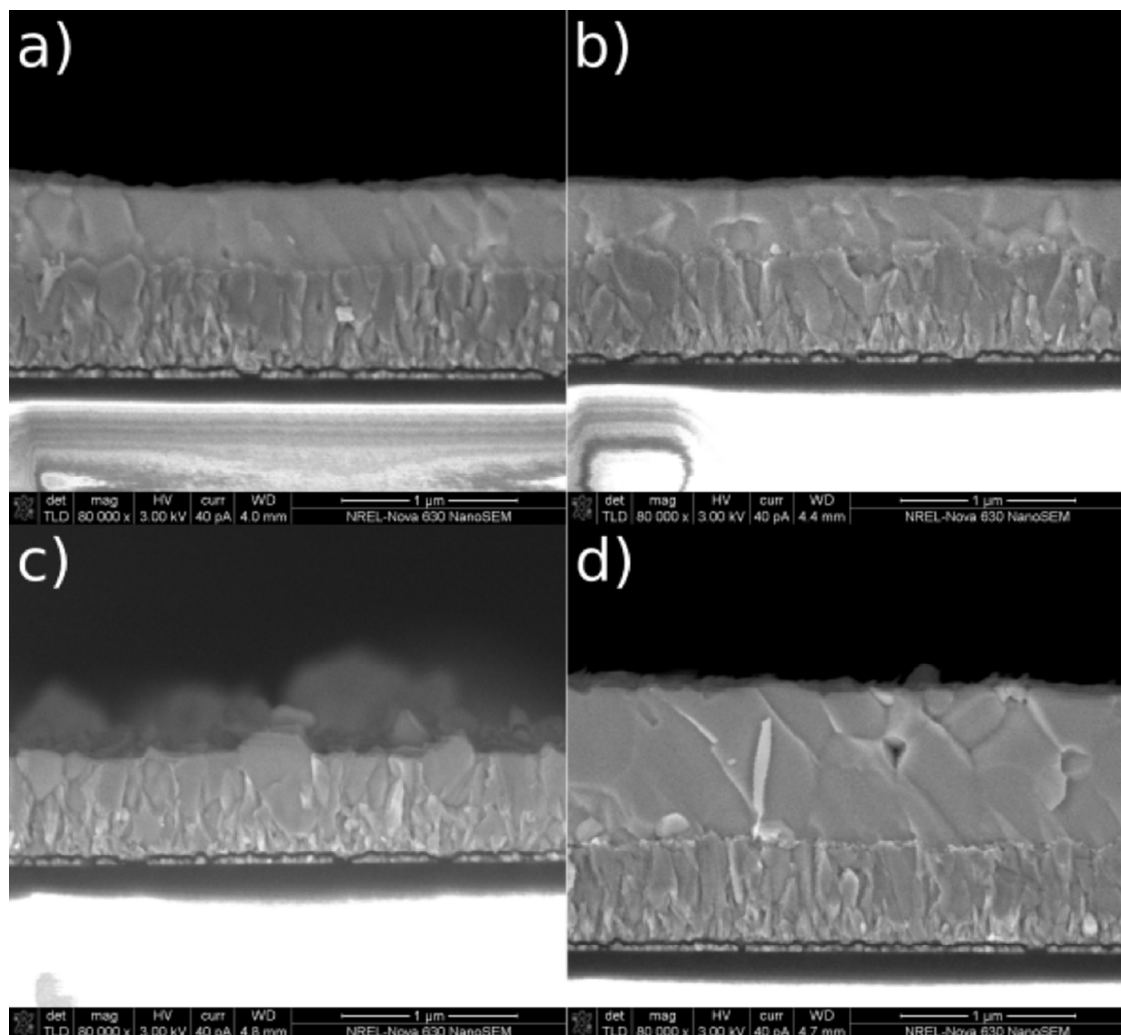


Figure S4. Cross sectional SEM images obtained for (a) FTO/SnO_x/MAPI pre-laminated half-stack, (b) FTO/NiO_x/MAPI pre-laminated half-stack, (c) FTO/SnO_x delaminated half, and (d) FTO/NiO_x/MAPI/MAPI delaminated half show that lamination causes structural evolutions to occur.

Time-resolved Photoluminescence (TRPL): Time-resolved photoluminescence spectroscopy measurements were performed using the time-correlated single photon counting technique. Excitation light was generated by a Fianium SC-450-PP laser operating with an average power of 15.5 μW at a repetition rate of 10 MHz and a wavelength of 450 nm selected by a Fianium

AOTF system. A 470 nm long pass filter was used to remove scattering from the excitation source. The emission was detected using a Hamamatsu streak camera with a wavelength range of 200-900 nm and response of < 20 ps. All samples were positioned with the glass side facing the incident excitation light. To compare traces, data was shifted and normalized so that maximal values of 1 occurred at $t = 0$ ns. Baselines were then subtracted, and data were truncated to eliminate the intensity-dependent region of the graph at $t < 20$ ns. Figure S5 shows data and corresponding single exponential fits. Figure S6 shows a comparison of residuals between a single-exponential and double-exponential best fit using data from the delaminated sample.

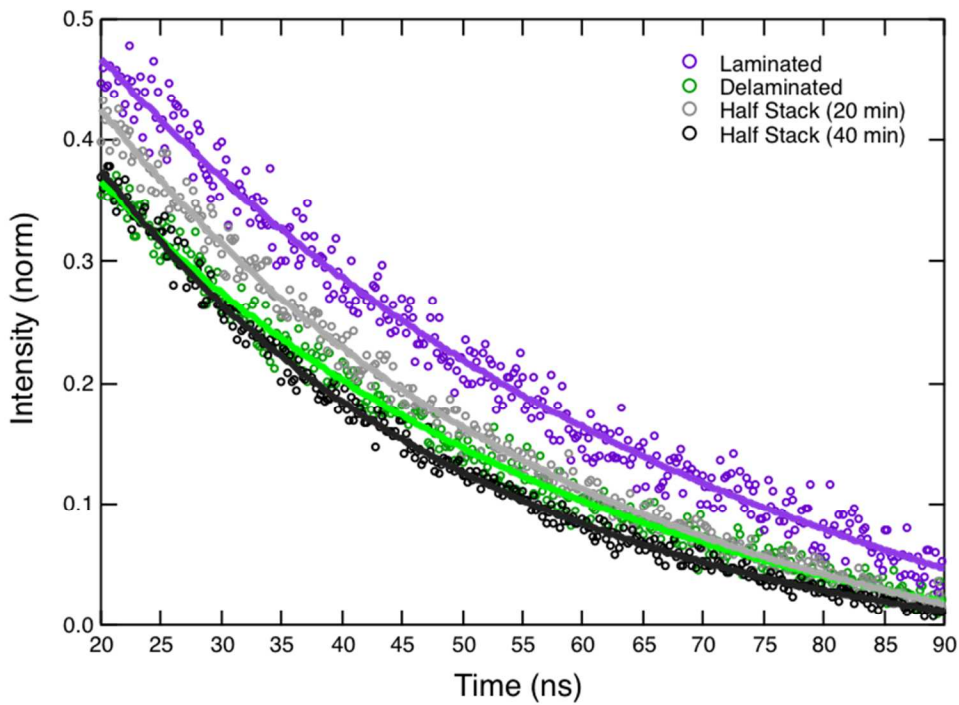


Figure S5. Time-resolved photoluminescence kinetics and corresponding single-exponential fits.

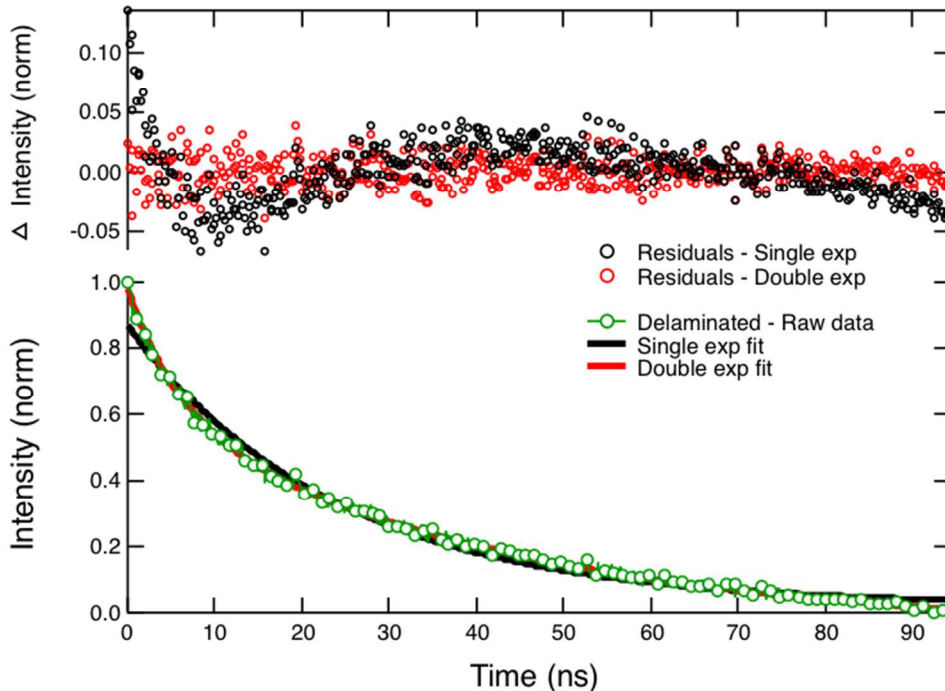


Figure S6. Single-exponential fit, double-exponential fit, and corresponding residuals for the time-resolved photoluminescence kinetics of the delaminated sample.

Device Characterization: $J-V$ curves were acquired in air with 100 mW/cm^2 AM1.5G illumination using a Newport 94083a Solar Simulator and Keithley 2400 Source Meter. The intensity of the solar simulator was calibrated using an encapsulated Si cell certified by the NREL Cell and Module Characterization group. Due to the discrepancy in active area size caused by the variable overlap of the two substrates in lamination, devices were masked using black electrical tape. Device areas were calculated in Image J using a high-resolution image of the cell and a ruler to determine area and calculate current density. Linear-sweep voltammetric scans were taken in the forward direction from -0.2 V to 1.2 V at a scan rate of 100 mV/s without prior bias or light soaking in ambient conditions.

Device controls: Given the novelty of the procedure presented, it is impossible to create a control device using the same chemistry as the laminated device. This is because both of the

transport layers must be deposited beneath the perovskite: the ETL due to solvent compatibility issues and the HTL due to thermal budgeting constraints. In order to provide a reference for the quality of the absorber, and our ability to produce high performance devices, we have included a representative curve from our standard, non-laminated device architecture (Figure S7).

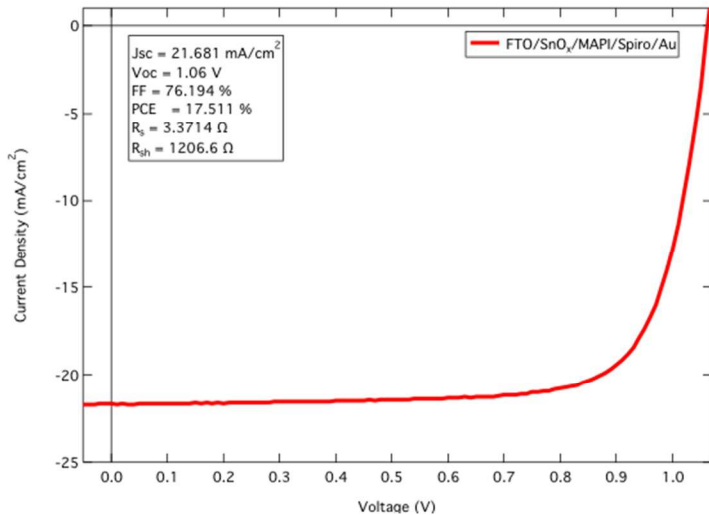


Figure S7. A FTO/SnO_x/MAPI/Spiro-OMeTAD/Au “control device” fabricated using the same MAPI recipe for the half stacks in the paper. The parameters of this device show that the MAPI layer resulting from minimizing PbI₂ is of high quality and produces efficient devices.

References

- (1) You, J.; Meng, L.; Song, T. Bin; Guo, T. F.; Chang, W. H.; Hong, Z.; Chen, H.; Zhou, H.; Chen, Q.; Liu, Y.; et al. Improved Air Stability of Perovskite Solar Cells via Solution-Processed Metal Oxide Transport Layers. *Nat. Nanotechnol.* **2016**, *11* (1), 75–81.
- (2) Jiang, Q.; Zhang, L.; Wang, H.; Yang, X.; Meng, J.; Liu, H.; Yin, Z.; Wu, J.; Zhang, X.; You, J. Enhanced Electron Extraction Using SnO₂ for High-Efficiency Planar-Structure HC(NH₂)₂PbI₃-Based Perovskite Solar Cells. *Nat. Energy* **2016**, *2* (1), 16177.
- (3) Noel, N. K.; Habisreutinger, S. N.; Wenger, B.; Klug, M. T.; Hörantner, M. T.; Johnston,

- M. B.; Nicholas, R. J.; Moore, D. T.; Snaith, H. J. A Low Viscosity, Low Boiling Point, Clean Solvent System for the Rapid Crystallisation of Highly Specular Perovskite Films. *Energy Environ. Sci.* **2017**, *10* (1), 145–152.
- (4) Dou, B.; Miller, E. M.; Christians, J. A.; Sanehira, E. M.; Klein, T. R.; Barnes, F. S.; Shaheen, S. E.; Garner, S. M.; Ghosh, S.; Mallick, A.; et al. High-Performance Flexible Perovskite Solar Cells on Ultrathin Glass: Implications of the TCO. *J. Phys. Chem. Lett.* **2017**, *8* (19), 4960–4966.
- (5) David Nečas, Petr Klapetek, Gwyddion: an open-source software for SPM data analysis, *Cent. Eur. J. Phys.* **2012**, *10* (1), 181-188.